JACS
JOURNAL OF THE AMERICAN CHEMICAL SOCIETY
Communication
pubs.acs.org/JACS

Molecular Mechanisms of Spin Crossover in the {Fe(pz)[Pt(CN)$_4$]} Metal–Organic Framework upon Water Adsorption

C. Huy Pham, Jordi Cirera,[†] and Francesco Paesani*

Department of Chemistry and Biochemistry, University of California, San Diego, La Jolla, California 92093, United States

Supporting Information

ABSTRACT: The rational design of multifunctional materials with properties that can be selectively controlled at the molecular level is key to the development and application of nanoscale devices. In this study, molecular dynamics simulations using ligand-field molecular mechanics are performed to elucidate, for the first time, the molecular mechanisms responsible for the variation of the spin-crossover properties of the {Fe(pz)[Pt(CN)$_4$]} metal–organic framework upon water adsorption. The simulations demonstrate a direct relationship between the water loading adsorbed in the pores and the variation of the spin-crossover transition temperature, with the high-spin state of the material becoming gradually more stabilized as the number of adsorbed water molecules increases. The decrease of the spin-crossover temperature of {Fe(pz)[Pt(CN)$_4$]} upon water adsorption predicted by the simulations is in agreement with the available experimental data and is traced back to the elongation of the bonds between the Fe(II) atoms and the organic linkers induced by interactions of the adsorbed water molecules with the framework.

The ability to control the physical and chemical properties of molecular assemblies at the nanoscale through the application of external stimuli is critical for the development of multifunctional materials, such as molecular switches, memory devices, and chemical sensors. By combining high porosity, large surface area, guest selectivity, and structural flexibility, metal–organic frameworks (MOFs) provide a promising platform for developing such stimuli-responsive materials.[1] MOFs are three-dimensional networks constructed by connecting metal ions or clusters (referred to as secondary building units or SBUs) with multidentate ligands.[2] Due to their intrinsic chemical diversity and porosity, MOFs have recently emerged as promising materials for several technological applications, including gas storage,[3] carbon capture,[4] hydrocarbon separation,[5] catalysis,[6] electrical,[7] and proton[8] conductivity.

The incorporation of SBUs containing open-shell transition metals results in MOFs that exhibit spin-crossover (SCO) behavior.[9−14] In these MOFs, the crystal field generated by the ligands removes the degeneracy of the metal d-based orbitals and, consequently, multiple spin states become available to each metal atom. If the energy gap (ΔE) between the nonbonding and antibonding sets of d-based orbitals is large compared to the pairing energy, the ground state of each open-shell transition metal corresponds to the low-spin (LS) state, while the high-spin (HS) state becomes the ground state if ΔE is small compared to the pairing energy. SCO may then occur in response to external perturbations (e.g., temperature or pressure changes and light irradiation).[15]

Since SCO transitions are accompanied by distinct changes in the physical properties of the framework (e.g., color, magnetism, and pore size), the synthesis of spin-crossover MOFs represents a major step toward the development of nanomaterials that can transform external stimuli into information signals. An example of this behavior is provided by the family of Hoffmann-type {Fe(pz)[M(CN)$_4$]} MOFs (pz = pyrazine, and M = Ni, Pd, Pt).[9] These materials display cooperative thermal- and light-induced SCO with transition temperatures ($T_{1/2}$) close to room temperature. Of particular interest is the {Fe(pz)[Pt(CN)$_4$]} MOF that exhibits bidirectional chemo-switching between LS and HS states upon adsorption of different guest molecules.[11] Specifically, while the SCO transition for the empty framework is centered at 295 K with a hysteresis of 24 K ($T_{1/2,\ down}$ = 285 K and $T_{1/2,\ up}$ = 309 K), the adsorption of protic solvents (e.g., alcohols and water) and bulky molecules (e.g., benzene and pyridine) stabilizes the HS state, shifting $T_{1/2}$ to lower values. In contrast, CS_2 molecules adsorbed in the MOF pores stabilize the LS state. No effect on the SCO transition is observed upon adsorption of small molecules such as CO_2 and N_2. Importantly, the {Fe(pz)[Pt(CN)$_4$]} MOF exhibits "memory effects", retaining a given spin state upon guest desorption.[11]

In this study, hybrid Monte Carlo/molecular dynamics (MC/MD) simulations combined with ligand field molecular mechanics (LFMM)[16] are used to elucidate the molecular mechanisms responsible for the variation of the SCO properties of {Fe(pz)[Pt(CN)$_4$]} upon water adsorption. Within LFMM,[17−19] conventional molecular mechanics energy expressions are supplemented with an additional term that effectively represents the ligand field stabilization energy arising from the splitting and different electron occupation of the metal d-based orbitals. The variation of $T_{1/2}$ for {Fe(pz)[Pt(CN)$_4$]} is investigated by performing a series of MC/MD simulations at different temperatures (from T = 100 K to T = 600 K) and different water loadings (from N_w = 1 to N_w = 5 water molecules per unit cell).[16] Specific details about the simulation protocol and the calculation of $T_{1/2}$ are described in the Supporting Information.

In Figure 1, the value of $\chi_M T$, with χ_M being the molar magnetic susceptibility of {Fe(pz)[Pt(CN)$_4$]}, calculated from the MC/MD simulations indicate a progressive shift of the SCO

Received: March 9, 2016
Published: May 5, 2016

DOI: 10.1021/jacs.6b02564
J. Am. Chem. Soc. 2016, 138, 6123−6126

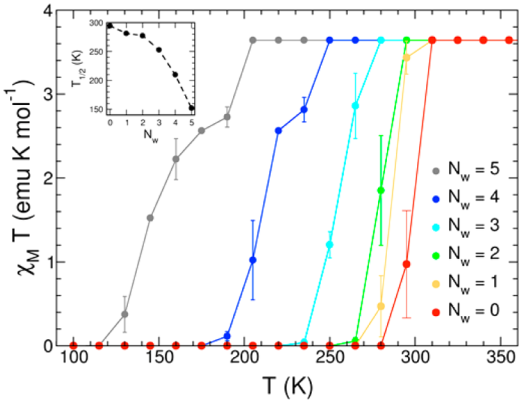

Figure 1. Temperature dependence of $\chi_M T$ calculated from hybrid MC/MD-LFMM simulations as a function of number of water molecules (N_w) adsorbed per unit cell. The corresponding values of the spin-crossover transition temperature ($T_{1/2}$) are shown in the inset.

transition to lower temperature as a function of water loading. However, the sequential adsorption of water molecules in the pores clearly has different effects on the SCO properties of the MOF material. As shown in the inset of Figure 1, a distinct change in the material response occurs at N_w = 2, with $T_{1/2}$ decreasing significantly more rapidly at higher loadings. Although up to 5 water molecules per unit cell can be adsorbed in {Fe(pz)[Pt(CN)$_4$]},[11] the SCO transition has been experimentally characterized only for N_w = 2. However, two different sets of experimental values have been reported ($T_{1/2,up}$ = 240 K and $T_{1/2,down}$ = 220 K in ref 9, and $T_{1/2,up}$ = 280 K, $T_{1/2,down}$ = 260 K in ref 20). The value predicted by the MC/MD simulations (277 K) is in excellent agreement with the latter experiment.

The dependence of $T_{1/2}$ on the number of water molecules adsorbed in the MOF pores can be directly related to the variation of the structural parameters of the framework. As shown in Figure 2a,c, the average bond distance between the Fe(II) atoms in the LS state and the N atoms of the pyrazine linkers is significantly shorter than the corresponding value calculated at high temperature, when the Fe(II) atoms are in the HS state. In addition, independently of the amount of water

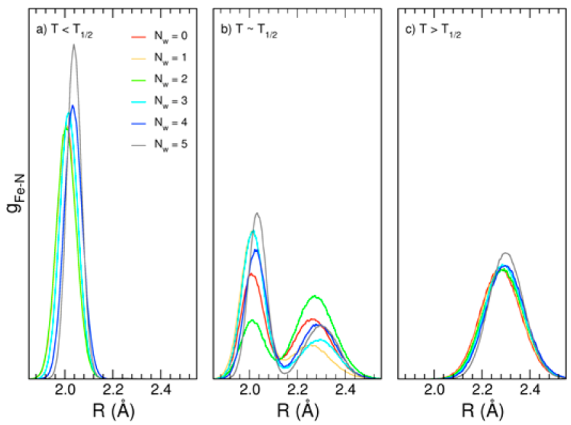

Figure 2. Distributions of the bond lengths between the Fe(II) atoms and the N atoms of the pyrazine linkers at temperatures below (a), close to (b), and above (c) the spin-crossover transition temperature $T_{1/2}$ calculated as a function of the number of water molecules (N_w) adsorbed per unit cell.

adsorbed in the pores, the distribution of the Fe−N bond distances becomes broader as the temperature increases. This is associated with the weakening of the Fe−N bonds in the HS state as a result of the electrons occupying the antibonding d-based orbitals. Of particular interest is the variation of the Fe−N bond distance in the LS and HS states as a function of N_w. When the Fe(II) atoms are in the LS state, the average Fe−N bond distance increases by ∼0.4 Å from N_w = 1 to N_w = 5. In contrast, independently of the amount of water adsorbed in the pores, the average Fe−N bond distance remains essentially constant when the Fe(II) atoms are in the HS state. A similar trend is found for the bond distances between the Fe(II) atoms and the N atoms of the cyanide linkers (see Supporting Information). Importantly, the MC/MD simulations correctly predict a larger elongation of the axial Fe−N bonds than the corresponding equatorial bonds, which is related to the Jahn−Teller distortion. The increased distance between the LS Fe(II) atoms and the ligands leads to an overall expansion of the framework, with a progressive stabilization of the HS state. The elongation of Fe−N bonds in the LS state directly correlates with the decrease of $T_{1/2}$ as the number of water molecules adsorbed in the pores increases. As shown in Figure 2b, the Fe−N bond distance distributions become bimodal as the temperature approaches $T_{1/2}$, providing evidence for the simultaneous presence of Fe(II) atoms in both LS and HS states within the framework.

Further insights into the physical mechanisms responsible for the variation of $T_{1/2}$ upon water adsorption are derived from the analysis of the spatial arrangements of the H_2O molecules inside the MOF pores (Figure 3a). The first water molecule adsorbed per unit cell is located near the center of the pore, with the H atoms being effectively aligned with the N atoms of the pyrazine rings and the O atoms almost equidistant from the eight metal atoms at the corners of the pore. As N_w increases, the water molecules begin to fill the available volume, establishing a fully connected hydrogen-bond network that propagates through the

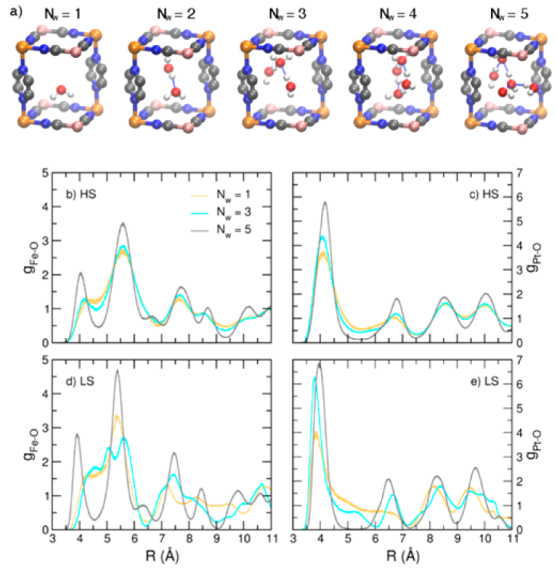

Figure 3. (a) Average positions of the water molecules inside the MOF pores calculated as a function of N_w. Color scheme: C atoms in dark gray, N atoms in blue, Fe(II) atoms in orange, and Pt(II) atoms in pink. (b,d) Fe−O and (c,e) Pt−O radial distribution functions describing the spatial correlations between the oxygen (O) atoms of the water molecules and the metal atoms (Fe and Pt) when the Fe(II) atoms are in the HS (b,c) and LS (d,e) states.

DOI: 10.1021/jacs.6b02564
J. Am. Chem. Soc. 2016, 138, 6123−6126

pores. As found in other MOFs,[21,22] the confining environment of the pores also has dramatic effects on the dynamical properties of the adsorbed water molecules (see Supporting Information).

More direct information on the water−framework interactions can be extracted from the analysis of the radial distribution functions (RDFs) describing the spatial correlations between the oxygen atoms of the water molecules (O) and the Fe(II) and Pt(II) atoms of the framework (Figure 3b−e). Minor differences are found for the same RDFs calculated with the framework in either the LS or the HS state, indicating that the pore expansion has negligible impact on how water molecules interact with the framework. Significant differences instead emerge when both Fe−O and Pt−O RDFs are analyzed as a function of N_w. The overall shape of the Pt−O RDFs is nearly independent of the number of water molecules present in the pores, displaying a pronounced peak at $R_{Pt-O} \approx 4.2$ Å and a series of lower peaks at larger separations that result from the translational periodicity of framework. In contrast, the Fe−O RDFs exhibit large variations as N_w increases, with the appearance of a well-defined peak at shorter distance ($R_{Fe-O} \approx 4.0$ Å) when the average number of water molecules per unit cell is larger than three. This specific feature, indicative of the development of stronger interactions between the water molecules and the Fe(II) atoms of the framework, directly correlates with the elongation of Fe−N bonds and, in turn, with the larger decrease of $T_{1/2}$ for $N_w > 2$. The analysis of the spatial distribution of H_2O molecules inside the {Fe(pz)[Pt(CN)$_4$]} pores, reported here for the first time, thus provides direct insights into the variation of the SCO properties in terms of the underlying water−framework interactions.

The present MC/MD simulations also enable, for the first time, the molecular-level characterization of the framework dynamics upon SCO transition. In particular, the simulations show that the SCO transition is accompanied by marked changes in the rotational mobility of the pyrazine rings (Figure 4). The different time scales associated with this rotational motion can be determined from the time decay of the orientational correlation function $C_2(t)$ defined in the Supporting Information. While the pyrazine rings undergo only low-amplitude librations below $T_{1/2}$ (Figure 4c), high rotational mobility is found at higher temperature, in agreement with quasielastic neutron scattering and solid-state ^{2}H NMR measurements (Figure 4b).[12] Since the MC/MD simulations predict that the pyrazine rings rotate faster, i.e., faster decay of $C_2(t)$, in the HS state than in the LS state at the same temperature (Figure 4d), the increased framework dynamics is not simply due to thermal activation but is directly related to the pore expansion in the HS state, which effectively provides the pyrazine rings with more room to undergo rotations. Importantly, the MC/MD simulations clearly show that the pyrazine rings do not undergo continuous rotations but perform discrete jumps between four orientations that are equally spaced by 90°, in agreement with the experimental observation of a 4-fold jump motion.[12] By filling the MOF pores, the sequential adsorption of H_2O molecules progressively suppresses the ability of the pyrazine rings to perform complete rotations (see Supporting Information). These results are in agreement with the experimental observation of restricted rotational motion of the pyrazine rings when bulky molecules are adsorbed in the pores.[11,12]

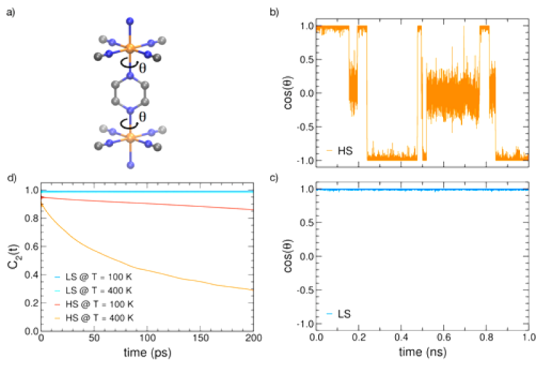

Figure 4. (a) Molecular model for the rotation of the pyrazine rings (by the angle θ) within the framework. (b) Time dependence of $\cos(\theta)$ in the HS state demonstrating the 4-fold jump motion. (c) Time dependence of $\cos(\theta)$ in the LS state demonstrating the absence of any rotational motion. (d) Time dependence of the function $C_2(t)$ in the LS and HS states at both low and high temperature demonstrating that the increased rotational mobility of the pyrazine rings is a consequence of the pore expansion in the HS state and is not simply due to thermal activation.

In summary, we have presented a systematic molecular-level analysis of the spin-crossover behavior of {Fe(pz)[Pt(CN)$_4$]} upon water adsorption through MC/MD simulations performed using the LFMM approach. It is found that the decrease of $T_{1/2}$ directly correlates with the spatial arrangements of the water molecules inside the pores and the consequent deformation of the framework. While the MOF unit cell at low water loadings remains effectively unchanged compared to that of the dehydrated material, the MC/MD simulations predict substantial structural modifications as the number of water molecules adsorbed in the pores increases. The unit cell progressively expands to accommodate additional water molecules, resulting in a volume increase of ∼3% when five water molecules are adsorbed per unit cell. The analysis of the structural and dynamical properties of the framework demonstrates that this pore expansion results in a progressive stabilization of the HS state, with a consequent decrease of $T_{1/2}$.

■ ASSOCIATED CONTENT

Supporting Information

The Supporting Information is available free of charge on the ACS Publications website at DOI: 10.1021/jacs.6b02564.

Specific details about the simulation protocol and the calculation of $T_{1/2}$, along with further analysis of the dynamical properties of both adsorbed water and frameworks (PDF)

■ AUTHOR INFORMATION

Corresponding Author

*fpaesani@ucsd.edu

Present Address

†Departament de Química Inorgànica and Institut de Recerca de Química Teòrica i Computacional, Universitat de Barcelona, Diagonal 645, 08028 Barcelona, Spain.

Notes

The authors declare no competing financial interest.

■ ACKNOWLEDGMENTS

This research was supported by the U.S. Department of Energy, Office of Science, under award No. DE-FG02-13ER16387, and used resources of National Energy Research Scientific Computing Center, which is supported by the Office of Science of the U.S. Department of Energy under Contract DEAC02-

DOI: 10.1021/jacs.6b02564
J. Am. Chem. Soc. 2016, 138, 6123−6126

05CH11231. We thank Mr. Shelby Straight for comments and suggestions.

REFERENCES

(1) Kitagawa, S.; Kitaura, R.; Noro, S.-i. *Angew. Chem., Int. Ed.* **2004**, *43*, 2334.
(2) *Metal-Organic Frameworks. Applications from Catalysis to Gas Storage*; Farrusseng, D., Ed.; Wiley-VCH Verlag: Weinheim, Germany, 2012.
(3) Getman, R. B.; Bae, Y. S.; Wilmer, C. E.; Snurr, R. Q. *Chem. Rev.* **2012**, *112*, 703.
(4) Britt, D.; Furukawa, H.; Wang, B.; Glover, T. G.; Yaghi, O. M. *Proc. Natl. Acad. Sci. U. S. A.* **2009**, *106*, 20637.
(5) Herm, Z. R.; Wiers, B. M.; Mason, J. A.; van Baten, J. M.; Hudson, M. R.; Zajdel, P.; Brown, C. M.; Masciocchi, N.; Krishna, R.; Long, J. R. *Science* **2013**, *340*, 960.
(6) Ma, L. Q.; Abney, C.; Lin, W. B. *Chem. Soc. Rev.* **2009**, *38*, 1248.
(7) Talin, A. A.; Centrone, A.; Ford, A. C.; Foster, M. E.; Stavila, V.; Haney, P.; Kinney, R. A.; Szalai, V.; El Gabaly, F.; Yoon, H. P.; Leonard, F.; Allendorf, M. D. *Science* **2014**, *343*, 66.
(8) Ramaswamy, P.; Wong, N. E.; Shimizu, G. K. H. *Chem. Soc. Rev.* **2014**, *43*, 5913.
(9) Niel, V.; Martinez-Agudo, J. M.; Muñoz, M. C.; Gaspar, A. B.; Real, J. A. *Inorg. Chem.* **2001**, *40*, 3838.
(10) Southon, P. D.; Liu, L.; Fellows, E. A.; Price, D. J.; Halder, G. J.; Chapman, K. W.; Moubaraki, B.; Murray, K. S.; Létard, J.-F.; Kepert, C. J. *J. Am. Chem. Soc.* **2009**, *131*, 10998.
(11) Ohba, M.; Yoneda, K.; Agusti, G.; Munoz, M. C.; Gaspar, A. B.; Real, J. A.; Yamasaki, M.; Ando, H.; Nakao, Y.; Sakaki, S.; Kitagawa, S. *Angew. Chem., Int. Ed.* **2009**, *48*, 4767.
(12) Rodríguez-Velamazán, J. A.; González, M. A.; Real, J. A.; Castro, M.; Muñoz, M. C.; Gaspar, A. B.; Ohtani, R.; Ohba, M.; Yoneda, K.; Hijikata, Y.; Yanai, N.; Mizuno, M.; Ando, H.; Kitagawa, S. *J. Am. Chem. Soc.* **2012**, *134*, 5083.
(13) Coronado, E.; Minguez Espallargas, G. *Chem. Soc. Rev.* **2013**, *42*, 1525.
(14) Aravena, D.; Castillo, Z. A.; Muñoz, M. C.; Gaspar, A. B.; Yoneda, K.; Ohtani, R.; Mishima, A.; Kitagawa, S.; Ohba, M.; Real, J. A.; Ruiz, E. *Chem. - Eur. J.* **2014**, *20*, 12864.
(15) Gutlich, P.; Garcia, Y.; Goodwin, H. A. *Chem. Soc. Rev.* **2000**, *29*, 419.
(16) Cirera, J.; Babin, V.; Paesani, F. *Inorg. Chem.* **2014**, *53*, 11020.
(17) Deeth, R. J. *Coordination Chemistry*; Springer: Berlin Heidelberg, 1995; Vol. *82*, p 1.
(18) Deeth, R. J. *Coord. Chem. Rev.* **2001**, *212*, 11.
(19) Deeth, R. J.; Anastasi, A.; Diedrich, C.; Randell, K. *Coord. Chem. Rev.* **2009**, *253*, 795.
(20) Delgado, T.; Tissot, A.; Besnard, C.; Guenee, L.; Pattison, P.; Hauser, A. *Chem. - Eur. J.* **2015**, *21*, 3664.
(21) Terranova, Z. L.; Agee, M. M.; Paesani, F. *J. Phys. Chem. C* **2015**, *119*, 18239.
(22) Paesani, F. *J. Phys. Chem. C* **2013**, *117*, 19508.

DOI: 10.1021/jacs.6b02564
J. Am. Chem. Soc. 2016, 138, 6123−6126